Journal of Applied Mechanical Engineering
ISSN: 2168-9873

Shi et al., J Appl Mech Eng 2015, 4:4
DOI: 10.4172/2168-9873.1000170

Research Article Open Access

The Finite Element Analysis and Optimization of an Elliptical Vibration Assisted Cutting Device

Guilin Shi[1], Chen Zhang[1]*, Yingguang Li[1], Kornel F Ehmann[2], Yun Song[1] and Ming Lu[1]

[1]*College of Mechanical and Electrical Engineering, Nanjing University of Aeronautics and Astronautics, China*

[2]*Department of Mechanical Engineering, Northwestern University, USA*

Abstract

The 2D elliptical vibration assisted cutting(EVC), which has significant advantages in the tool wearing restriction, cutting heat reduction, the quality of the finished surface improvement, is widely supposed to be the most promising machine method to difficult-to-cut materials and micro-texturing formation. Based on the certain 2D EVC structure, three structures of different angles (30°, 60°and 90°) for optimization and the corresponding finite element models of the three structures are created. The simulation analyses of static structure, modal and harmonic response of these structures have been conducted. The 60° topological structure was selected for the final design model after the comprehensive comparison about the resonance frequency, vibration modes and vibration amplitudes of the elliptical trajectories in the tool tip. The performance test system has been established for the testing of the actual 2D EVC device, and the comparison analyses between the results of finite element analysis and the experiment results have been detailed. The experimental data showed that the optimized structure could generate the required elliptical locus for the elliptical vibration cutting. Comparing with the finite element analysis results, the guidance effect of the finite element analysis method to the structure optimization and trajectory prediction has been successfully verified.

Keywords: Elliptical vibration; Cutting; Finite element analysis; Optimization

Introduction

As the fast development of the micro machine in recent years, micro-texturing has attracted more and more attention in research and application. Comparing with laser ablation, LIGA and the other means of micro-texturing formation, the EVC (elliptical vibration assisted cutting) technology has many advantages in terms of costing, efficiency and time saving, which is becoming more and more popular in surface micro topography fields [1]. The EVC technology was first introduced by Hong and Ehmann [2], it adds the vibration to the tool tip in depth of cut direction and cutting direction, which would bring better cutting effect to the finished surface [3,4]. The current research showed the performance of the micro-texturing is determined by its shapes and distribution style [5], but the EVC was mainly focus on keeping the vibration of the tool tip stable to obtain a single shape, which restricted the EVC application in the micro fields [6]. Ping and Kornel have developed an EVC device [7], which has been verified successfully in the ultrasonic micro-texturing machine, but the shapes of texturing are single micro-grooves. For all the above reasons, in this paper the authors have designed three structures of different angles based on the structure and kinematic analysis of Ping's EVC device, then the simulations of vibration and deformation have been conducted.

Finite element method (FEM) analysis has been proved significantly useful in prediction by simulation in the field of vibration assisted cutting. Amini studied the machining forces and stresses acting on the work piece during the ultrasonic assisted turning by FEM analysis [8]. Lu has developed finite element models to analyze the effect of vibration frequency on cutting forces and cutting temperature during elliptical vibration turning [9]. Vivekananda has used FEM in the calculation of the natural frequency and amplitude of EVC device in his work [10], and later he has proved the optimization effect of FEM in process parameters selection [11]. Huang enhanced the cutlery life and drilling process quality by investigating the micro drill's natural properties by FEM [12].

In this paper, FEM is firstly used for the performance optimization (including resonance frequency, vibration amplitude, and etc.) of the 2D EVC structure, and then the actual EVC device based on the optimization is manufactured for the following experiment [13]. The corresponding theoretical model of the tool tip trajectory is established and the elliptical locus is proved. The comparisons between the experimental data and the simulation data are detailed in the aspects of excitation amplitude and phase difference. The predictability and the reliability of the created finite element model are verified by the comprehensive comparisons.

Principle and Dynamic Analysis of the EVC Structure

Principle and of EVC and the EVC structure

The work piece surface is selected to be the reference for the illustration of the EVC principle. As shown in Figure 1, the cutting trajectory (dash-line) left on the work piece surface is contributed by the synthesis of the tool's vibration and the work piece's rotation. During the machine, different from the tool constant contacting with the work piece in conventional cutting, EVC creates the separation intermittent between the tool and the work piece, which is advantageous for the heat dissipation, the wearing suppression and longer tool life. The elliptical trajectories of the tool edge left on the work piece forms the required micro-texturing finally.

***Corresponding author:** Chen Zhang, College of Mechanical and Electrical Engineering, Nanjing University of Aeronautics and Astronautics, China, Tel: +86 25 8489 2899; E-mail: meeczhang@nuaa.edu.cn

Received August 04, 2015; **Accepted** August 21, 2015; **Published** August 28, 2015

Citation: Shi G, Zhang C, Li Y, Ehmann KF, Song Y, et al. (2015) The Finite Element Analysis and Optimization of an Elliptical Vibration Assisted Cutting Device. J Appl Mech Eng 4: 170. doi:10.4172/2168-9873.1000170

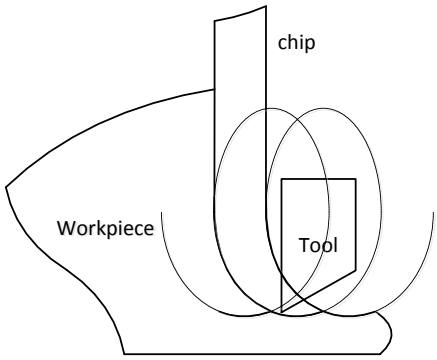

Figure 1: Principle of the EVC.

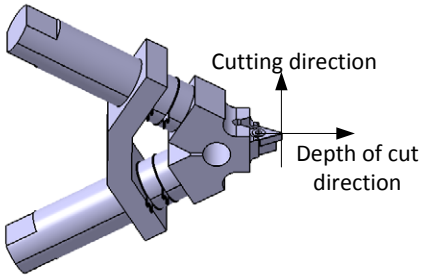

Figure 2: CAD model of the EVC structure.

The CAD model of the EVC structure studied in this paper is showed in Figure 2. This structure is composed by two Langevin transducers which are fixed on the base by bolts. The header works as the tool holder and synthetizes the two transducer's displacement to the tool. When the excitations applied on the two transducers are in the same phase, the transducers' movements in the cutting direction are cancelled out by each other for the symmetry of the structure, the tool tip moves along the depth of cut direction; when the excitations are in the opposite phase, the transducers' movements in the depth of cut direction are cancelled out by each other and the tool tip moves along the cutting direction. In the recent research, EVC has two work modes, which are resonant mode and non-resonance mode. By the common sense, the amplitude of the EVC in the resonant mode is several times or even more than which in the non-resonance mode. In the fields of micro-texturing, the big amplitude provides the EVC with a broad range of elliptical locus, which is advantageous to the diversification of the micro-texturing. As the consequence, in this paper, the resonant work mode is selected for the FEM simulation and the actual experiments.

Kinematic analysis of the 2D EVC equipment

The principle of the elliptical vibration formation of the EVC equipment used in this paper is shown in Figure 3. For the convenience of the specification, some simplification is been made with the main structure unchanged. The excitations applied on the two transducers have the same amplitude and frequency, the phase difference is 90°, as shown in Figures 3 and 4. Figure 5 is the tool's positions correspond to the different phases in Figure 3. The transducers are separately named as rod A and rod B as shown in Figure 4. The position of the tool is contributed by the two Langevin transducers' displacements. Assuming one vibration cycle begins at the point whose phase value is a (in the next paper, phase a, is short for this point) in Figures 2 and 3, at this moment, the displacements of rod A and rod B have the same displacement. To the tool tip, the horizontal components (the cutting direction in Figure 4) are cancelled out by the structures' symmetry, and the vertical components (the depth of cutting direction) superimpose each other. In the whole vibration locus, the position of the tool tip in phase a is on the peak in depth of cut direction. In phase b, rod B displacement reaches the small position with the rod A position unchanged, the tool tip reaches the left limit of the locus. The positions in phase c and d are the same as in phase a and b, when the tool run to the phase a' in next round cycle, the whole elliptical vibration is completed. Adjust the excitation frequency to the resonance mode, the bigger amplitude achieved and the device can be used for the actual experimental cutting.

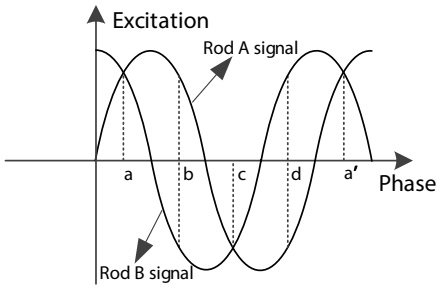

Figure 3: Excitation signals applied on the transducers.

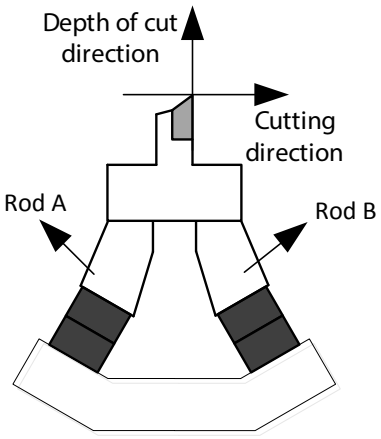

Figure 4: Illustration of rods and directions.

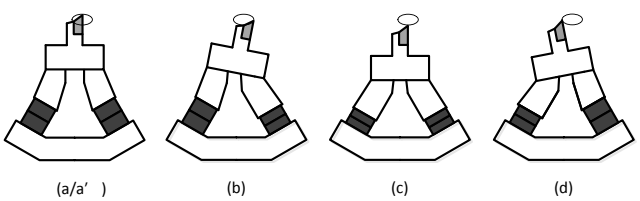

Figure 5: Generation of the elliptical trajectory in the tool tip.

Based on the conclusion above, the EVC equipment in this paper is mainly influenced by the two transducers' amplitudes and phase differences, the elliptical locus can be modified by controlling the two factors. The following content analysis the relations between the amplitudes and phase differences and the tool tip elliptical locus, the results is verified in experiments.

Mathematical model of the trajectory at the tool tip

Based on the analyses above, the mathematical model of the trajectory of the tool tip is established as shown in Figure 6a. The transducers are named as rod A and rod B, and the amplitude of each other is A and B, the angle between the rods is θ, the frequencies is the same and represent as F, the phase difference is φ, t is time. In the initial condition (without any excitation input), PD_0 is the point of the tool tip, PM_0 is the middle point of the simplified connection rod, PA_0 and PB_0 is the endpoint of rod A and rod B separately. θ_D is the angle between the line from PM_0 to PD_0 and the horizontal line, can be calculated by $\theta_D = \tan^{-1}(\frac{T}{L})$.

For the kinematic model created above, at time t, the position of tool tip point $PD_t(pd_x, pd_y)$ in two directions (ox and oy) can be formulated into Equation (1).

$$\begin{cases} pd_x = pm_x - \sqrt{L^2+T^2}\cos(\theta_t - \theta_D) \\ pd_y = pm_y - \sqrt{L^2+T^2}\sin(\theta_t - \theta_D) \end{cases} \quad (1)$$

In the Equation (1), as shown in Figure 6b where T is the thickness of the tool, L is the distance between PD and the connection rod. $D$is the length from PB_0 (or PA_0) to, $PM_0\theta_t$ is the angle between the tool holder and the horizontal line at time t, PM_t is the middle point of the connection line at time t, pm_x and pm_y are the corresponding coordinates. Considering the symmetric of the structure, pm_x and pm_y can be formulated in to Equations (2) (Figure 7).

$$\begin{cases} pm_x = \dfrac{pa_x + pb_x}{2} \\ pm_y = \dfrac{pa_y + pb_y}{2} \end{cases} \quad (2)$$

In the Equation (2), where pa_x and pa_y are the coordinates of, PA_t. pb_x and pb_y are the coordinates of PB_t.$PA_t$and PB_t. are the endpoints of rod A and rod B at time t separately.

The rods are excited by the sinusoidal signals in Figure 3, $pa_x$and pa_y can be formulated in to Equations. (3).

$$\begin{cases} pa_x = pa_{0x} - A\sin(2\pi ft)\cos(\dfrac{\theta}{2}) = -A\sin(2\pi ft)\cos(\dfrac{\theta}{2}) \\ pa_y = pa_{0y} - A\sin(2\pi ft)\sin(\dfrac{\theta}{2}) = D - A\sin(2\pi ft)\sin(\dfrac{\theta}{2}) \end{cases} \quad (3)$$

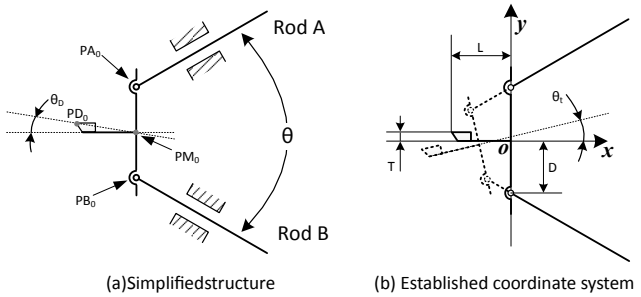

(a)Simplifiedstructure (b) Established coordinate system

Figure 6: Kinematic model of the tool tip vibration.

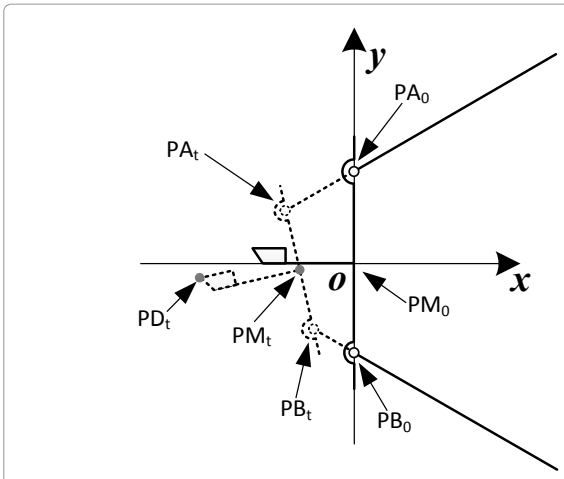

Figure 7: Illustration of representation.

In the Equation (3), wherepa_{0x} and $pa_{0y}$are the coordinates of PA_0, as the given parameters, $pa_{0x} = 0, pa_{0y} = D$. Equation (4) shows the coordinates of $PB_t(pb_x, pb_y)$, the formula reasoning procedure will not be repeated for its similarity with PA_t.

$$\begin{cases} pb_x = pb_{0x} - B\sin(2\pi ft+\varphi)\cos(\dfrac{\theta}{2}) = -B\sin(2\pi ft)\cos(\dfrac{\theta}{2}) \\ pb_y = pb_{0y} + B\sin(2\pi ft+\varphi)\sin(\dfrac{\theta}{2}) = D + B\sin(2\pi ft)\sin(\dfrac{\theta}{2}) \end{cases} \quad (4)$$

The coordinates of PD_t and θ_t can be obtained by substituting the intermediate variables as shown in Equation (5) and (6).

$$\begin{cases} pd_x = \dfrac{-A\sin(2\pi ft)\cos(\frac{\theta}{2}) - B\sin(2\pi ft+\varphi)\cos(\frac{\theta}{2})}{2} - \sqrt{L^2+T^2}\cos(\theta_t - \theta_D) \\ pd_y = \dfrac{-A\sin(2\pi ft)\sin(\frac{\theta}{2}) + B\sin(2\pi ft+\varphi)\sin(\frac{\theta}{2})}{2} - \sqrt{L^2+T^2}\sin(\theta_t - \theta_D) \end{cases} \quad (5)$$

$$\theta_t = \frac{\pi}{2} + \tan^{-1}\left(\frac{2D - A\sin(2\pi ft)\sin(\frac{\theta}{2}) - B\sin(2\pi ft+\varphi)\sin(\frac{\theta}{2})}{-A\sin(2\pi ft)\cos(\frac{\theta}{2}) + B\sin(2\pi ft+\varphi)\cos(\frac{\theta}{2})}\right) \quad (6)$$

In this paper, the amplitudes$A$ and B are equal, the phase difference is 90°. To a certain structure, L, T, θ_D are constant. The position of the tool tip can be simplified as follows:

$$\begin{cases} pd_x = \dfrac{-A\sin(2\pi ft)\cos(\frac{\theta}{2}) - A\cos(2\pi ft)\cos(\frac{\theta}{2})}{2} - \sqrt{L^2+T^2}\cos(\theta_t - \theta_D) \\ pd_y = \dfrac{-A\sin(2\pi ft)\sin(\frac{\theta}{2}) + A\cos(2\pi ft)\sin(\frac{\theta}{2})}{2} - \sqrt{L^2+T^2}\sin(\theta_t - \theta_D) \end{cases} \quad (7)$$

During the simplification of the formulas, $-\theta_D$ substitutes $\theta_t - \theta_D$ for $\theta_t \ll \theta_D$, then the position equations can express as:

$$\begin{cases} \dfrac{pd_x + \sqrt{L^2+T^2}\cos(-\theta_D)}{-\frac{A}{2}\cos(\frac{\theta}{2})} = \sin(2\pi ft) + \cos(2\pi ft) \\ \dfrac{pd_y + \sqrt{L^2+T^2}\sin(-\theta_D)}{-\frac{A}{2}\sin(\frac{\theta}{2})} = \sin(2\pi ft) - \cos(2\pi ft) \end{cases} \quad (8)$$

The sum (9) of the squaring of Equation (8) is a standard ellipse equation with the center coordinate being $(-\sqrt{L^2+T^2}\cos(-\theta_D), -\sqrt{L^2+T^2}\sin(-\theta_D))$, the length of the semi-major axis being $(\frac{A}{\sqrt{2}}\cos(\frac{\theta}{2}))$ and the length of the semi-minor axis being $(\frac{A}{\sqrt{2}}\sin(\frac{\theta}{2}))$.

$$\left(\frac{pd_x+\sqrt{L^2+T^2}\cos(-\theta_D)}{\frac{A}{\sqrt{2}}\cos(\frac{\theta}{2})}\right)^2+\left(\frac{pd_y+\sqrt{L^2+T^2}\sin(-\theta_D)}{\frac{A}{\sqrt{2}}\sin(\frac{\theta}{2})}\right)^2=1 \quad (9)$$

Finite Element Analyses of the 2D EVC Devices

The piezoelectric ceramics convert the electrical energy to the mechanical energy when the EVC works in physical condition, namely simple harmonic motion can be achieved by the transduces when the excitations are sine waves. The preload of the device implied on the PZT rings makes the vibration transfer to the whole device, as well as the tool tip. As the consequence, the elliptical vibration can be obtained on the tool tip. Considering the efficiency and necessaries, the simulation won't directly perform on the PZT's output performance, the amplitude is getting by the experimental parameters and functions, and the excitation used in the finite element analysis is imported as the displacement. In another word, during the finite element analysis to each device, the input parameters are the displacement amplitudes, frequency and the phase difference, the parameters and calculation functions are given in the following section.

Preparing for the simulation

The displacement amplitudes of PZT under inverse piezoelectric effect can be calculated by the following formula [10]:

$$\delta = n \bullet d_{33} \bullet U_3 \quad (10)$$

In the formulas, where n is the quantity, d_{33} is the coefficient in direction, U_3 is the voltage amplitude. The$d_{33}$of the PZT used in this paper is 220×10^{-12} m/V. The voltage amplifier has the bipolar range of 0 to ± 350 V, and the slew rate is 500 V/us which are enough to the experiment. The single transducer is composed of two mechanical series PZT rings which are parallel connected in circuit, so the value of n is 2. The displacement amplitude of the PZT in the above condition can be calculated as follows:

$$\delta = 2\times350\times220\times10^{-12} = 15.4\times10^{-8} m \quad (11)$$

The devices of three different common angles are shown in Figure 8 (a is θ=30° , b is θ=60° , c is θ=90°), whose main structures remain unchanged. The following section studies the influence of the angles to the tool tip's trajectory.

The simulations in this paper are performed in ANSYS Workbench (in the next, WB is short for it). There are three main steps for common simulations analysis in WB, which include the foundation of the model, the meshing grid and the post processing. Considering the complexity

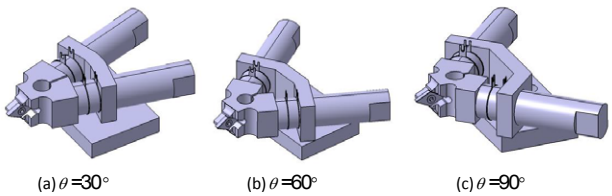

(a) θ=30° (b) θ=60° (c) θ=90°

Figure 8: CAD models of different angles.

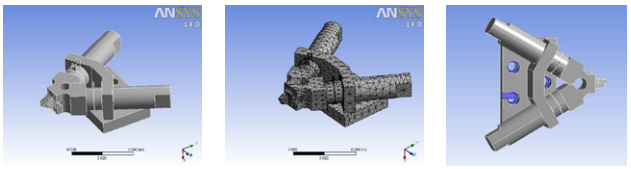

(a)import the model (b)mesh grid (c) constrains and loads

Figure 9: Processes of the simulation in WB.

of the model creating in WB and the compatibility to IGES (the general 3D type data), the models of the structures are created in CATIA, saved as igs files and then imported to WB.

Modal analysis is adopted to confirm the nature frequency and vibration modes of the structure in common kinematic simulation, and the results can also provide the other kinematic analysis (the harmonic response analysis, random vibration analysis, etc.) parameters with reference. Harmonic response confirms the structures' steady state response in the loads whose amplitudes and frequency are already known. Harmonic response includes two kinds of transient dynamic analysis, linear and non-linear. The former is suitable for small strain and stress of the model structure and the linear analysis also has two algorithms which are direct way and mode suppression. Considering the property of the device in this paper, the linear analysis and mode suppression algorithm are selected for the FEA simulation.

When to the simulation in WB of ANSYS, after the running of the soft and establishing the analysis program, import the model of IGS to the program by the interface provided by WB, as shown in Figure 9a, the model is imported successfully. For the fully understand of the kinematic property of the structure, set the grid mesh accuracy to medium by the smart mesh Figure 9b. The fixed constrains are applied on the torus of counter bores surfaces in the bottom of the model Figure 9c. The theoretical results of the PZTS's output are applied on the structure as the amplitudes of excitations.

Modal and harmonic response analyses

The harmonic responses are separately performed to the three structures by the method of mode suppression in the same condition (the material, the constrains and loads and the grid meshing). For the convenience of data comparison, the amplitudes (in cutting direction and depth of cutting direction) of simulation results of the three structures are shown in one figure. The comparison of the amplitudes in depth of cutting direction of different structures is shown in Figure 10. The range of the frequency is 0 to 50 kHz and the step size is 500 Hz.

As shown in Figure 10a, in terms of the depth of cut direction, there are obvious differences in resonance frequency and amplitude between different structures. The 30° structure has a bigger amplitude in high frequency, and resonances in 13 kHz, 35 kHz, 35 kHz, and reaches the peak amplitude of 2.72 μm in 44.4 kHz; the 30° structure has the superiority in the range of low frequency comparing with the other structures except some certain frequency point and reaches the amplitude peak 3.43 μm in 6 kHz; the 90° structure has a relative minor amplitude in the whole simulation range.

For clearly comparing of the amplitudes of three structures in different vibration modes, Figures 10b and 11 are made for comparison. In these two figures, the value in horizontal axes is the vibration mode order.

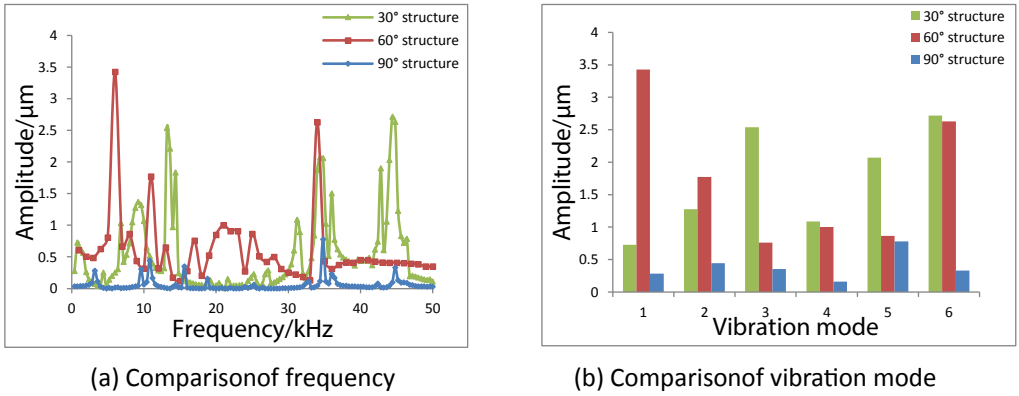

Figure 10: Influence of frequency on the amplitude in depth of cut direction.

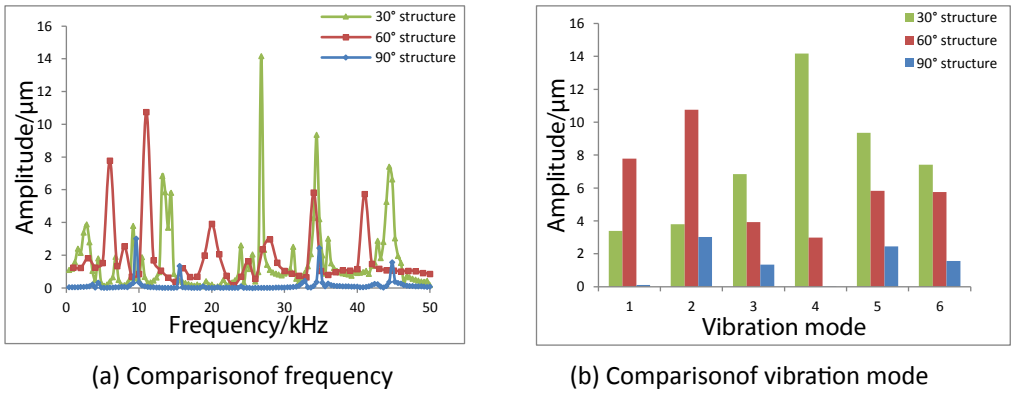

Figure 11: Influence of frequency on the amplitude in cutting direction.

In terms of the amplitudes in cutting direction of the tool tip, 30° structure reaches the amplitude peak 14.165 μm in 26.8 kHz and resonances at 13 kHz, 34.4 kHz, 44.4 kHz; 60° structure reaches the amplitude peak 10.753 μm in 11 kHz and resonances at 6 kHz, 20 kHz, 34 kHz, 41 kHz; 60° structure has the obvious shortage in amplitude except some certain frequency when compare to the other two structures (Table 1).

As seen from the comparisons above, in both depth of cut direction and cutting direction, the 90° structure has a clear defection in amplitude comparing to the other two structures, which is disadvantage to the following operation. When to the 30° structure, there are some superiorities in amplitudes in some certain frequency (34.4 kHz, 44.4 kHz), but in a certain frequency range, there are some vibration modes combine together, which can be seen in figure as the extreme points in a small frequency range. These gather may lead to the instability of the trajectory of the tool tip, which is harmful to the machine accuracy, and the manufacture error of the structure may even deteriorate this phenomenon. The vibration modes distribution of 60° structure are discrete in the simulation range which can avoid the instability when physical machine theoretically.

Stress and strain analysis

The stress finite element analyses are simulated to verify if the intensity of the vibration structure meet the stiffness requirements. Figure 12a is the structure's strain cloud chart and Figure 12b is the stress cloud chart. As shown in the figure, the strain of the structure reaches the maximum in the tool tip, which is agreed with the design objective.

θ/°		30	60	90
Vibration stability[1]	Depth direction[2]	0.26	0.14	0.2
	Cutting direction	0.34	0.2	0.12
Average amplitude[3]/μm	Depth direction	1.737	1.742	0.392
	Cutting direction	7.418	6.17	1.411
Average resonance frequency[4]/kHz	Depth direction	22.13	19	21.33
	Cutting direction	21.8	23.33	23.66

[1]Vibration stability is ratio of the number of extreme points and the number of the whole simulation points, the higher the ratio value is, the lower stability the structure performs.

[2]Depth direction is short for depth of cut direction.

[3]Average amplitude is the average value of amplitudes of the former six vibration modes.

[4]Average resonance frequency is the average value of the former six vibration mode frequencies.

Table 1: Comprehensive comparison of three structures.

The stress concentration occurs in the flexible hinge (Figure 12b), which may exceed the fatigue limit of the material. So the detailed discussion of the structure stress in flexible hinge is given in the following. The stress in flexible hinge in different excitation frequency is shown in Figure 13. The red line in the figure represents the allowable

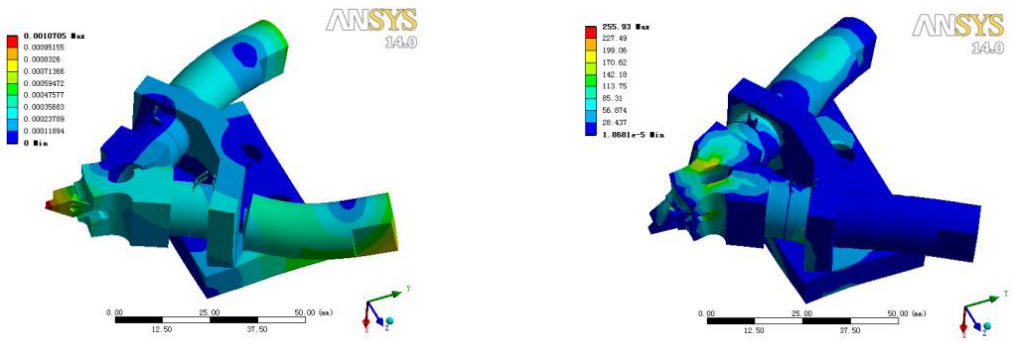

(a) Strain cloud (b) Stress cloud

Figure 12: Strain and stress cloud of the structure.

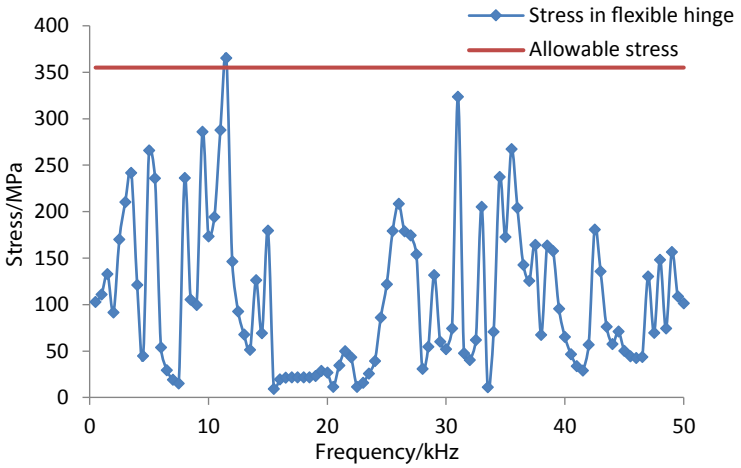

Figure 13: Stress in flexible hinge in different frequency.

stress (350 MPa) of the material; the blue line is the stress in flexible hinge by different frequency. The figure clearly shows that, except the point of 11.5 kHz, the stress is under the allowable stress, which means the structure meets the requirements in the stress field in most frequency.

As the consequence, considering the consequence performance (amplitudes, stability and stress) of three structures, the 60°structure is finally adopted for the following manufacturing and physical experimental testing.

Experiment and Comparison

Experiment condition

Figure 14 shows the experiment condition, the material is 45# steel. The signals are generated by Data Acquisition Card which is programed by LABVIEW on PC, then amplified by the power amplifier which has a 0 ± 350 V bipolar output. The two Langevin transducers are excited by the outputs of the amplifier. The displacements of the tool tip are measured by the Micro Sense capacitance sensors and processed by the Data Acquisition Card. The displacement data are shown in real time by the LABVIEW and recorded as LVM files in PC for post processing.

Frequency response tests

The frequency response data of the tool tip in experimental is also recorded and analyzed. The voltage amplitude applied on the PZT in this experiment is 350 V. Comparing with the simulation results (Figures 15 and 16), there is a certain difference between the theoretical and experimental results. Figures 15a and 16a show the comparison of amplitude in depth of cut direction and cutting direction separately. The analyses of the differences in resonance frequency and amplitude are given in the following section.

The comparison of the simulation and experimental results are shown in Figure 15b, the resonance frequencies of the physical device basically consistent with the simulation results but a little deviation; the amplitudes differences are much more apparent in the figure and the simulation results are less than the experimental results, this is may possibly cause by the PZT's calibration coefficient error. The amplitudes in 23 kHz and 29 kHz are much bigger than common, this may cause by the manufacture and assembly error.

In terms of amplitudes in cutting direction of the tool tip, the trends of two results are basically in accordance with each other. As shown in Figure 16b, the experimental results verify most of the simulation

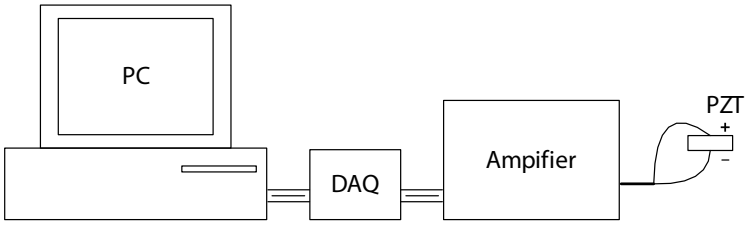

Figure 14: Experiment condition.

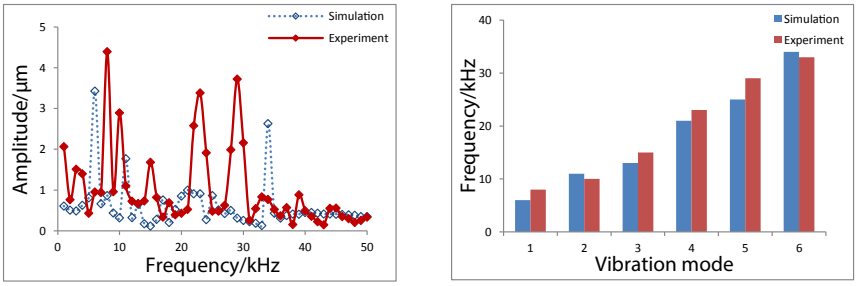

(a) Comparisonof frequency (b) Comparisonof vibration mode

Figure 15: Simulation and experiment comparison in depth of cut direction.

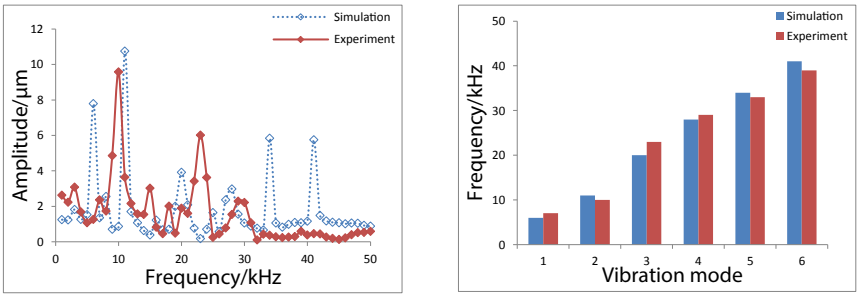

(a) Comparisonof frequency (b) Comparisonof vibration mode

Figure 16: Simulation and experiment comparison in cutting direction.

prediction with a little deviation. At the same time, the great decrease in amplitude of the experimental vibration mode in 34 kHz and 41 kHz cannot be neglected.

From the analyses above, it can be obviously seen that in the low frequency range (0-20 kHz), the simulations make a good agreement with the experiments, when to the high frequency range (above 33 kHz), the deviations arise to the extent which cannot be ignored, which provides little reference for the experiments.

Excitation phase difference tests

In Figure 3, the phase of the excitation applied on rod B is 1/4 cycle time earlier than which applied on rod B, the direction of the elliptical locus at the tool tip is clockwise which can be used for EVC machine. The simulations show that the excitation phase differences have an effect on the elliptical motion of the tool tip in both amplitude and direction, which means in some phase difference range, the device is not suitable for EVC. Simulations and corresponding experimental tests of this effect are conducted and the results are discussed in the following.

The experimental results under the effect of the phase differences are solid line in blue color in next two figures (Figures 17 and 18), and the simulation results are dash line in red color. The trends of the amplitude changes of the tool tip in depth of cut direction and cutting direction are in consistent, when the phase difference is 160°, the maximum amplitude in both directions achieved, and 320° the minim amplitude achieved. The cycle of the tool tip vibration is the same as the simple harmonic excitations' cycle.

Figure 17 shows the comparison of the amplitudes in the depth of cut direction of the tool tip trajectory between simulations and experimental results influenced by the phase difference. Except a certain difference in the amplitudes in some certain points, the simulation results match the experimental results well in both varying trends and specific values.

In terms of the amplitudes in cutting direction in the elliptical trajectory of the tool tip, as shown in Figure 18, the trend of the variation of amplitude in the simulation matches the experimental data well, the corresponding values can also consistent with which measured in the

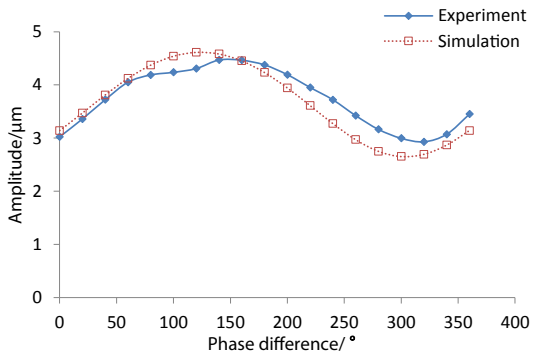

Figure 17: Simulation and experiment comparison in depth of cut direction amplitude.

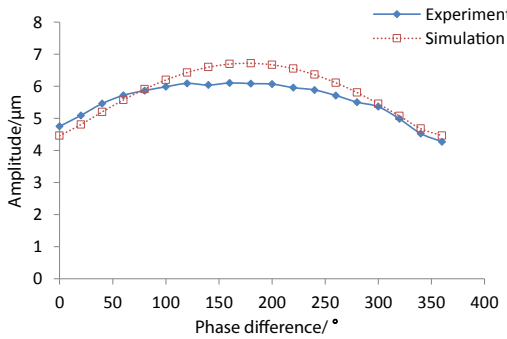

Figure 18: Simulation and experiment comparison in cutting direction amplitude.

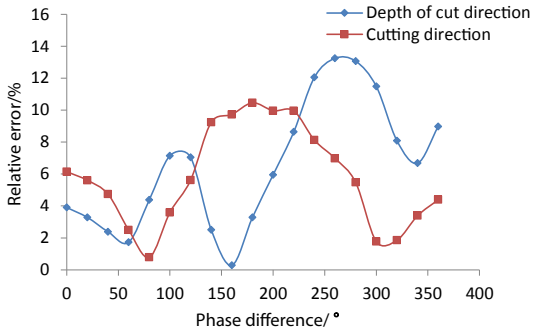

Figure 19: Relative error between simulation and experiment.

experiments considering a certain error.

As shown in the two figures (Figures 17 and 18), no matter in the depth of cut direction or in the cutting direction, the variation trends of the amplitudes by the phase difference are both apparent in either simulations or experiments, and two trends exactly consistent with each other. To the amplitude values in a certain phase difference, for the clear comparing, the figure about the error between the simulation and experimenting two directions is shown in Figure 19. The value of the relative error in Figure 19 is calculated as the following formula (12):

$$\text{Relative error} = \frac{\text{simulation data-experiment data}}{\text{experiment data}} \quad (12)$$

As shown in this the figure, the error is under 10% in most phase difference, which is acceptable considering the factors of the environment effect, simplification and device manufacturing. The

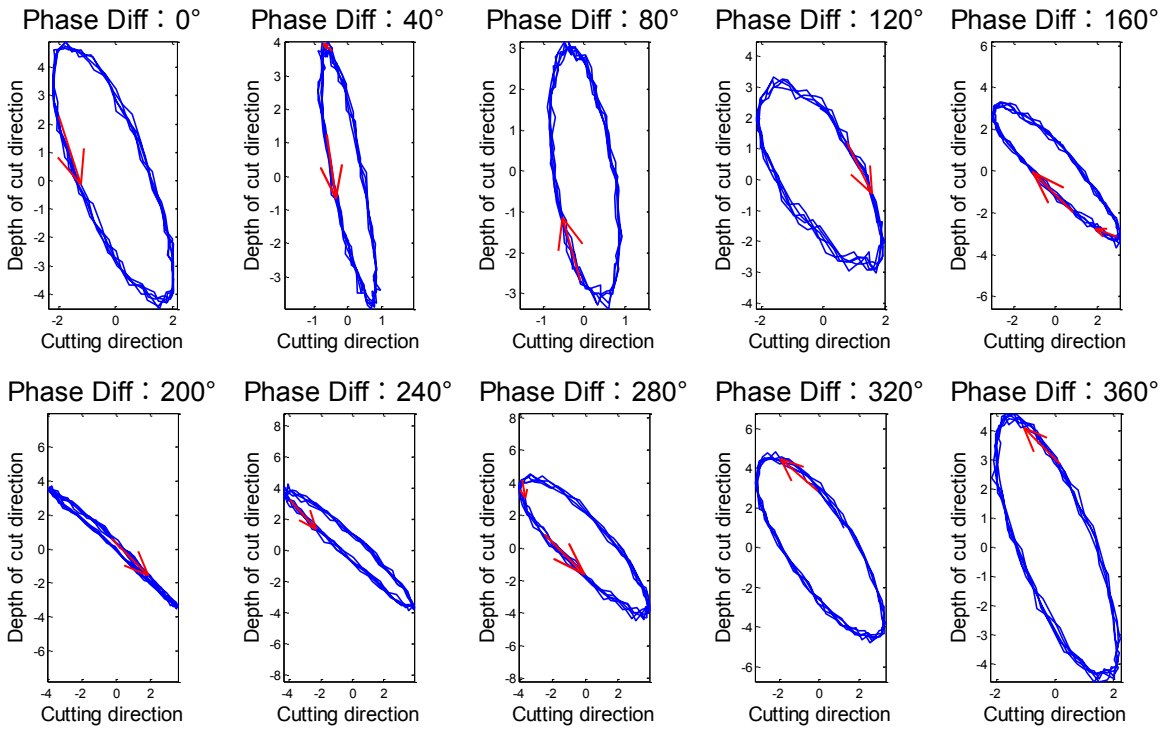

Figure 20: Influence of phase difference on the trajectory.

error in both directions is basically in the same trend, but in the phase difference range 120°-280°, the error in depth of cut direction goes through with a peak while the other with a valley. During this range, the error in depth of cut direction reaches the maximum 10.46% when the phase difference is 180°, and the error in cutting direction reaches minimum 0.29% when the phase difference is 160°. In the whole phase difference cycle, the maximum error in depth is 13.25% at 260°, and the minimum error in cutting direction is 0.78% at 80°.

To the structure placed by the means in this paper (Figure 4), only when the tool tip moves along the clockwise direction, the tool works in EVC condition. Figure 20 shows in effect of the phase difference to the direction of the tool's trajectory. The amplitude of the excitation voltage is 350 V.

As shown in the figure, the tip moves in the anticlockwise direction when the phase difference in the range of 0° to 60°and 240° to 360°, which cannot be used for EVC machine; when the phase difference in the range of 60° to 240°, the tool tip moves in clockwise direction, which can be used for EVC machine. When the phase difference close to the boundary (60° and 240°), the minor axis of the elliptical locus decreases to zero, the locus nearly becomes a straight line in a certain phase difference, then the move direction of the tool tip changes as the phase difference increases furtherly.

From the Figure 20, when the phase difference changes, the slope of the elliptical trajectory of the tool varies. When the phase difference is 90°, the major axis of elliptical trajectory approximately along the depth of cut direction. The slope increases when the phase difference away from 90°. When the phase difference reaches 180°approximately, the slope reaches the maximum, after then the slope decrease with the phase difference increasement until the next cycle.

Conclusion

Based on the structure analysis and kinematic analysis of an EVC device, FEM is used for a serious simulations includes locus amplitudes of the tool tip, the resonance frequency and the vibration modes in different angles of device. After comprehensive comparison of the simulation results, the 60° structure is selected for the final optimization. The actual device is manufactured by the optimization and tested in a series of experiments, the simulation results are verified by the experimental data. The comparison shows that, ignoring a certain manufacture and measurement errors, the simulation models established in this paper can optimize the vibration structure and predict the locus of the tool tip successfully, which make a significantly meaning to the wide application of the EVC device in the following research.

References

1. Zhang J, Suzuki N, Wang Y, Shamoto E (2014) Fundamental investigation of ultra-precision ductile machining of tungsten carbide by applying elliptical vibration cutting with single crystal diamond. Journal of Materials Processing Technology 214: 2644-2659.
2. Hong MS, Ehmann KF (1995) Generation of engineered surfaces by the surface-shaping system. International Journal of Machine Tools and Manufacture 35:1269-1290.
3. Zhang JG, Suzuki N, Kato T, Hino R, Shamoto E (2012) Influence of material composition on ductile machining of tungsten carbide in elliptical vibration cutting. In Key Engineering Materials 523: 113-118.
4. Arif M, Rahman M, San WY (2011) Analytical model to determine the critical feed per edge for ductile–brittle transition in milling process of brittle materials. International Journal of Machine Tools and Manufacture 51: 170-181.
5. Ziki JDA, Didar TF, Wüthrich R (2012) Micro-texturing channel surfaces on glass with spark assisted chemical engraving. International Journal of Machine Tools and Manufacture 57: 66-72.
6. Kim GD, Loh BG (2007) An ultrasonic elliptical vibration cutting device for micro V-groove machining Kinematical analysis and micro V-groove machining characteristics. Journal of materials processing technology 190:181-188.
7. Guo P, Ehmann KF (2013) Development of a tertiary motion generator for elliptical vibration texturing. Precision Engineering 37: 364-371.
8. Amini S, Soleimanimehr H, Nategh MJ, Abudollah A, Sadeghi MH (2008) FEM analysis of ultrasonic-vibration-assisted turning and the vibratory tool.Journal of materials processing technology 201: 43-47.
9. Lu D, Cai LG, Cheng Q (2014) Finite Element Study of Ultrasonic Elliptical Vibration Turning of Ti6Al4V. Applied Mechanics and Materials 494: 383-386.
10. Vivekananda K, Arka GN, Sahoo SK (2014) Finite element analysis and process parameters optimization of ultrasonic vibration assisted turning (UVT). Procedia Materials Science 6: 1906-1914.
11. Vivekananda K, Arka GN, Sahoo SK (2014) Design and Analysis of Ultrasonic Vibratory Tool (UVT) Using FEM and Experimental Study on Ultrasonic Vibration-assisted Turning (UAT). Procedia Engineering 97: 1178-1186.
12. Huang BW, Chen WT, Tseng JG (2015) Finite Element Analysis on Natural Properties of a Micro Drill with Ultrasonic Vibration. Applied Mechanics and Materials 764: 285-288.
13. Jaffe B (2012) Piezoelectric ceramics. Elsevier.